Experimental Studies of Spontaneous and Forced Transition on an Axisymmetric Body

J.T. Kegelman* and T.J. Mueller†
University of Notre Dame, Notre Dame, Indiana

An experimental investigation of spontaneous and forced transition on a secant-ogive-nose axisymmetric body was conducted for length Reynolds numbers between 0.315×10^6 and 1.03×10^6. Several different transition modes were observed and documented using smoke-flow visualization and hot-wire anemometry. Sound was used to control the frequency and enhance the amplitude of the disturbances in the boundary layer during the forced transition studies. Three different mechanisms of transition originate as a viscosity-conditioned Tollmien-Schlichting (T-S) instability. The evolution of these instability waves depends upon Reynolds number and the frequency and amplitude of the disturbance. A change in the nonlinear development of the secondary instability—the Λ-vortex structure—could be induced by changing only the amplitude of the T-S waves, keeping all other conditions constant. The frequency spectra from a hot wire placed in this flowfield show an abrupt decrease in the psd of the subharmonic of the T-S wave frequency as the amplitude of the disturbance is increased. Mean and fluctuating velocity profiles and the mean pressure distribution along the body are also presented. The results support recent theories that describe the events in the nonlinear region.

Nomenclature

C	= phase velocity, $=\omega_i/\alpha$
C_p	= pressure coefficient, $=(P-P_\infty)/q$
D	= diameter of cylindrical section, equal to 1 caliber (10.16 cm)
L	= total length of axisymmetric body
P_e	= static pressure along model, N/m^2
q_∞	= freestream dynamic pressure
Re_δ, Re_L	= Reynolds number based on displacement thickness and total body length, respectively
U_∞	= freestream velocity
U_e	= local freestream velocity
x,y	= coordinate axes in freestream and azimuthal directions, respectively
z	= coordinate axis normal to body surface
α,β	= dimensionless wave numbers in x and y directions, $=(2\pi/\lambda_x)(x/\sqrt{Re_x})$ and $(2\pi/\lambda_y)(x/\sqrt{Re_x})$, respectively
δ,δ^*,θ	= boundary-layer, displacement, and momentum thicknesses, respectively
λ	= wavelength
μ,ν	= absolute and kinematic viscosity, respectively
ρ	= air density
ω_i	= dimensionless frequency, $=2\pi f(\nu/U_e^2)$

Introduction

RECENTLY, several investigations[1-5] have been conducted in an attempt to develop a better understanding of the transition processes on axisymmetric bodies, see for example, Fig. 1. These investigations primarily involved visualization of the transition process using smoke photography and high-speed motion pictures. The primary objective of the present investigation was to clarify and extend these earlier qualitative investigations by hot-wire-anemometer studies in regions where smoke photographs showed interesting fluid mechanical behavior, allowing more accurate interpretation of the visual data. In addition, the present investigation focused in part on the region of nonlinear development of Tollmien-Schlichting (T-S) waves. In the nonlinear region, spanwise variations of T-S wave amplitude lead to the peak-valley deformation of T-S waves as described by Klebanhoff et al.,[6] yielding Λ-shaped vortices prior to the breakdown to turbulence. The results presented herein, obtained on an axisymmetric body with a widely varying pressure gradient, complement recent theories[7-9] which attempt to improve the characterization of events that occur in the nonlinear region. Similar observations have been made in flat-plate boundary-layer experiments,[10-13] where the vibrating ribbon technique was used to generate and control T-S wave development. The results presented here were obtained using acoustic excitation on a realistic flight vehicle.

Craik[7] developed the triad theory in which the formation of Λ vortices is related to a remarkably strong nonlinear mechanism involving resonant interactions among a triad of T-S waves. Craik examined the relevance of the triad theory to the experiments of Klebanhoff et al.,[6] noting that further experimental work was needed to detect the presence of such triads. Craik's model predicts subharmonic resonance for wave triads with a specific spanwise wavelength λ_y. In several experimental investigations,[10-13] subharmonic frequencies along with the successive formation of harmonics were observed, while in the work of Klebanoff, et al.[6] only the main frequency and higher harmonics of similar intensities were observed. The appearance of subharmonics is clearly related to the mode in which the Λ vortices form. If Λ vortices form such that the peaks are aligned in the streamwise direction (i.e., the peaks follow peaks and valleys follow valleys), the Klebanoff mode, or K type, of instability is present. If the Λ vortices are in a staggered formation (i.e., peaks follow valleys), then a subharmonic appears that is associated with the passage of a peak in every other T-S wave. In several experiments the observed spanwise wavelength was found to disagree with the predictions of the Craik model.

An analysis by Volodin and Zelman[8] suggested three different paths for development of nonlinear waves depending on the initial character of the disturbance field. If the amplitudes

Presented as Paper 84-0008 at the AIAA 22nd Aerospace Sciences Meeting, Reno, NV, Jan. 9-12, 1984; received Feb. 29, 1984; revision received May 28, 1985.

*Research Assistant. Presently, Research Scientist, McDonnell Douglas Research Laboratories, St. Louis, MO. Member AIAA.

†Professor, Department of Aeronautical and Mechanical Engineering. Associate Fellow AIAA.

of all disturbances are equal, a rapid nonlinear growth of all synchronized fluctuations takes place. In flows where one frequency is stronger than all others, a nonlinear self-interaction becomes the dominant mechanism, yielding a transition process similar to that observed by Klebanoff et al.,[6] with a large number of harmonics and without the growth of subharmonics. In an intermediate case, where a single dominant frequency is present in the initial disturbance field but is not of significantly larger amplitude than the background disturbances, a subharmonic develops along with the higher harmonics.

The experimental observations of spanwise wavelengths that disagree with Craik's model led to an excellent analytic treatment of secondary instabilities developed by Herbert[9] for plane Poiseuille flow and which has recently been applied to the Blasius boundary layer. Herbert's analysis uses the fact that a neutral two-dimensional wave appears as a steady periodic motion when viewed from a frame moving with the phase velocity of the two-dimensional wave. A linear stability analysis of the three-dimensional, spanwise periodic disturbances then yields a system of differential equations with periodic coefficients. For Blasius flow, Herbert assumed that the shape of its finite-amplitude disturbances are similar in shape to the solutions given by the linear (infinitesimal disturbances) Orr-Sommerfeld theory. Herbert's numerical calculations show that a broad band of spanwise wave numbers associated with disturbance growth are possible, with the highest growth factors for low T-S wave amplitudes occurring where $\beta/\alpha \approx 0.65$. The synchronized triads of T-S waves (Craik's mechanism) are an integral part of the subharmonic instability mechanism. The results presented here support Herbert's theory, although his analysis was for the flat-plate Blasius boundary layer.

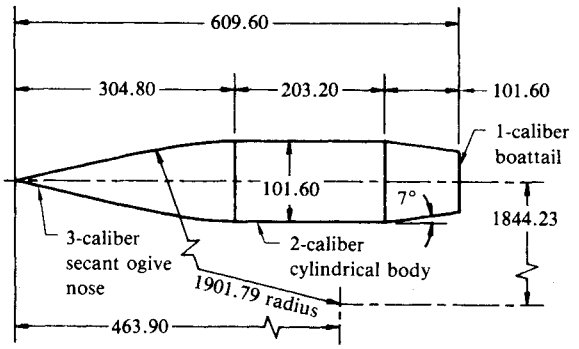

Dimensions in millimeters

Fig. 1 Flow-visualization model for the baseline secant ogive nose.

Test Facility

The experiments presented here were conducted in the University of Notre Dame's low-turbulence smoke wind tunnel shown in Fig. 2. The tests were conducted with flow velocities 5-27 m/s and a turbulence intensity of approximately 0.10% over the velocity range. Smoke was generated by a device that allowed deodorized kerosene to drop onto electrically heated plates. A detailed description of these facilities and their development can be found in Ref. 14.

A constant-temperature anemometer (DISA 55m10) was used to determine the model boundary-layer velocity and turbulence-intensity profiles as well as the turbulence-intensity levels in the test section. All hot-wire measurements were made with a 5-μm platinum-tungsten hot-wire probe (DISA 55P26). Boundary-layer surveys were accomplished using an automated traversing mechanism with a resolution of 0.1 mm in the freestream direction and 0.01 mm across the boundary layer. Frequency measurements were made at the point in the boundary layer where the disturbance amplitude was found to be a maximum. Sound disturbances were introduced upstream of the first antiturbulence screen, and care was taken to ensure that only a single frequency, free of harmonics, was introduced into the test section.

Results and Discussion

Although data were taken over a rather narrow range of Reynolds numbers—3.15×10^5 to 1.03×10^6 based on model length—the phenomena occurring on this model varied dramatically. At the lowest Reynolds number, the flow remained laminar over the entire body as shown in Fig. 3. The flow over the boattail was separated and, about 0.75 caliber down the boattail, axisymmetric vortex rings became visible in the smoke and were shed periodically into the wake.

Boundary-layer-velocity and turbulence-intensity profiles were taken every 25.4 mm along the model and every 2.54 mm in the separated region along the boattail. The velocity profiles for $Re_L = 3.15 \times 10^5$, shown in Fig. 4, also indicate that a laminar boundary layer exists along the entire length of the model, with the exception of the boattail. The turbulence-intensity profiles show that low levels of turbulence within the boundary layer, on the order of 0.2% U_∞, with the exception

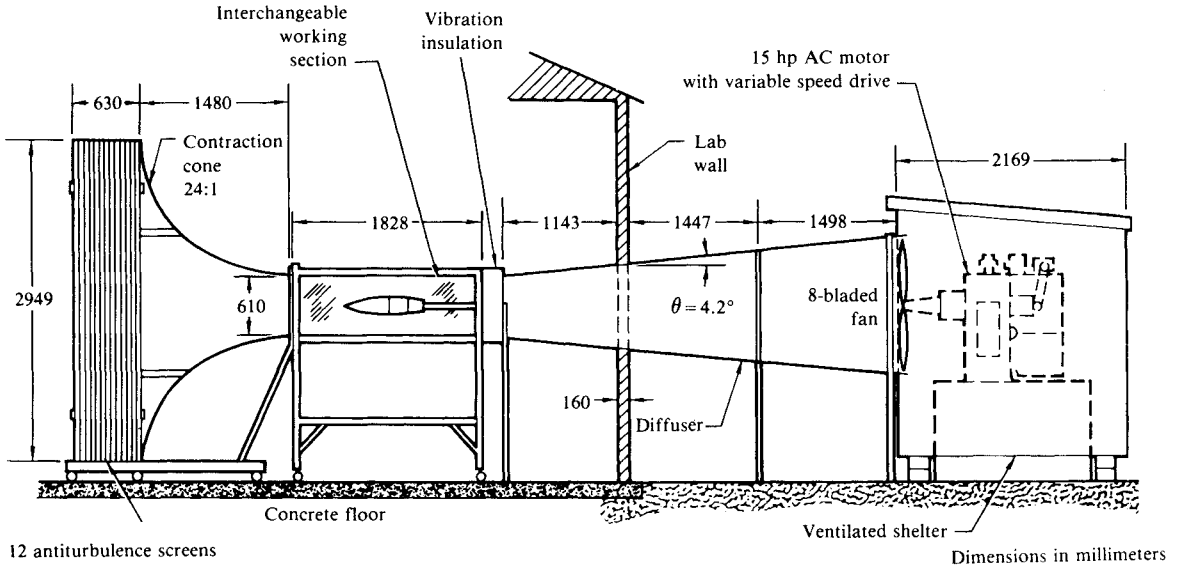

Dimensions in millimeters

Fig. 2 Low-turbulence subsonic smoke tunnel with axisymmetric body.

of the first few stations along the nose and in the separated regions along the boattail. The turbulence intensity is as high as 1.0% near the tip of the model and decays to 0.4% by the center of the ogive nose. This phenomenon results from the amplification of disturbances in the freestream as it approaches the stagnation point at the nose of the model. Similar boundary-layer profile measurements were made at $Re_L = 0.631$, 0.814, 0.928, and 1.04×10^6 and can be found in Ref. 15.

The velocity profiles along the boattail agree with visual observations, indicating that separation occurs almost immediately after the midsection boattail junction. For $Re_L = 3.15 \times 10^5$, the separated region appears to be 0.4-mm thick at the first station along the boattail, 2 mm downstream of the second shoulder. The turbulence-intensity profiles in the separated region show a significant turbulence level, $0.8\% U_\infty$, just behind the midsection/boattail junction. The turbulence-intensity dissipates further downstream until station 23 where it increases dramatically, reaching its maximum approximately at the point of inflection in the velocity profile. The smoke photographs and high-speed motion pictures indicate a rapid development of vortex rings at this point, consistent with the turbulence-intensity profiles along the boattail. Turbulence intensity is maximum at the end of the boattail, where the flow moves into the wake region.

The shedding frequency could be dramatically influenced by sound over a wide range of frequencies (as low as 40 Hz and as high as 270 Hz). For any frequency in this range and at moderate sound levels, the shedding frequency was the same as the sound frequency. Moderate sound levels were those registering about 90- to 100-dB sound pressure level at a microphone in the test section, using a one-third-octave bandpass filter tuned to the frequency of the sound. This separated shear layer, although close to a wall, is much like a free shear layer, being receptive to sound over almost three octaves. At the lowest frequencies, the wavelength of the activity along the boattail was as long as 25 mm, yielding a ratio of wavelength to boundary-layer thickness of about 8. At these low frequencies and at very high sound levels, the vortex rings deformed before leaving the boattail. A Λ-vortex-like structure occasionally was visible after deformation of the vortex rings, indicating a similarity to the events in the breakdown of the T-S waves. At these low frequencies, the wavelengths of the vortex rings have been forced by the sound to be much larger than the height of the separation bubble. Thus the ratio of wavelength to boundary-layer thickness is within the range of that for the T-S waves. At frequencies above 60 Hz, no Λ vortices could be formed, regardless of sound amplitude. Tollmien-Schlichting waves occasionally became visible on the midsection; however, the waves were visible only at low frequencies and extremely high sound levels (approximately 120 dB).

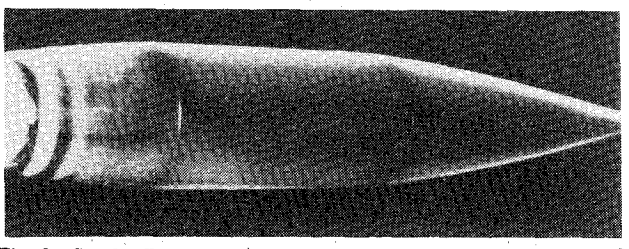

Fig. 3 Smoke-flow visualization over the model at $Re_L = 3.15 \times 10^5$.

Data were taken to document the frequency content in the shedding along the boattail when sound was introduced into the flow. When no sound was introduced, the hot wire did not detect any dominant frequency in the flow at station 22, halfway down the boattail, as illustrated by the rather flat frequency plot of Fig. 5a. Also, no vortex formation was visible in the smoke photographs at this point. When 42-Hz sound was introduced, the frequency spectra of the hot-wire signal, as shown in Fig. 5b, contained a strong spike at 42 Hz, as well as spikes at harmonic frequencies of 126, 210, 294, and 380 Hz. (If f is 42 Hz, these harmonics are $3f$, $5f$, $7f$, and $9f$.) When sound at a frequency of 267 Hz was introduced, the hot-wire signal again contained substantial power at the fundamental frequency, with harmonics at $2f$ (534 Hz) and $3f$ (801 Hz), as shown in Fig. 5c. Higher harmonics appear to be masked by the background noise. It is not clear at this time why the boundary layer develops harmonics of $3f$, $5f$, $7f$... when low frequencies are introduced and harmonics of $2f$, $3f$... when high frequencies are introduced.

At a Reynolds number of 814,000, two-dimensional T-S waves formed continuously at the midpoint along the body and disappeared (continuously) just before the boattail, as illustrated in Fig. 6. It has been shown in the numerical streakline simulation by Saric et al.[11] that when T-S waves

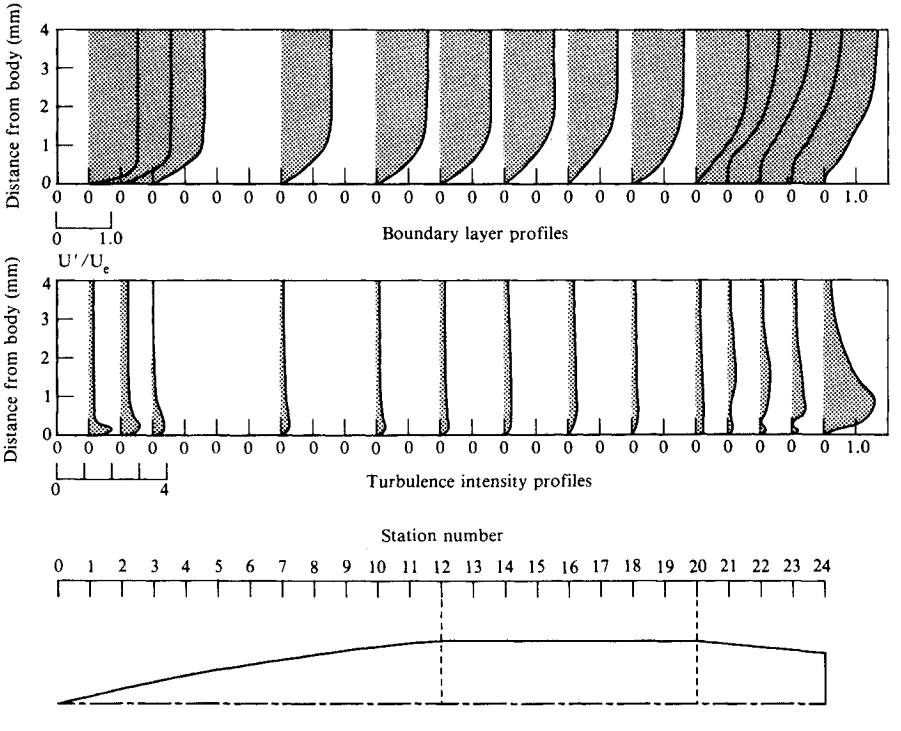

Fig. 4 Boundary-layer and turbulence-intensity profiles for $Re_L = 3.15 \times 10^5$.

decay in a favorable pressure gradient, the "cats-eyes" formations tend to become flattened and streaklines tend to merge. The disappearance of T-S waves in the smoke along the midsection is consistent with these streakline computations. In general, the shedding frequency along the boattail was not the same as the T-S wave frequency along the midsection. However, when sound was used to enhance the amplitude of the T-S waves, the vortex shedding frequency became the same as the T-S waves.

Figure 7 illustrates the spontaneous transition that occurs along the midsection of the model at the highest Reynolds number, 1.03×10^6. Groups of 2-5 two-dimensional waves became unstable and formed Λ vortices, almost simultaneously, indicating that a strong nonlinear mechanism is present. Approximately 90% of the Λ vortices appeared in a staggered formation, with 10% in an aligned formation.

The T-S wavelength, as well as the Λ-vortex wavelength and mode of formation (either aligned or staggered), could be dramatically influenced by both the frequency and amplitude of disturbance. During preliminary testing of the influence of sound on the boundary layer, it was observed that the T-S wavelength could be varied from approximately 8 mm at 1200 Hz to approximately 21 mm at 460 Hz. Extensive hot-wire measurements and visual observations were made at $Re_L = 8.14\times10^5$, since two-dimensional waves would appear and then disappear along the midsection, without any sign of three-dimensional deformation when no sound was used. Furthermore, two significantly different three-dimensional deformations were observed when sound was used to enhance the amplitude of the T-S waves at $Re_L = 8.14\times10^5$. Figures 8 and 9 show the response of the boundary layer to sound at 500 and 1000 Hz, respectively.

Neutral stability curves were generated using a stability code developed by Cebeci and Bradshaw.[16] The experimental boundary-layer profiles could not be used as input for the stability code because any slight nonuniformity due to experimental uncertainty would cause vastly misleading results. For this reason, boundary-layer profiles were generated numerically and used as input for the stability code. A comparison of the experimental and numerical boundary-layer profiles is shown in Fig. 10. The boundary-layer code used as input, measured pressure distribution shown in Fig. 11 as well as the body geometry and Reynolds number. Since the

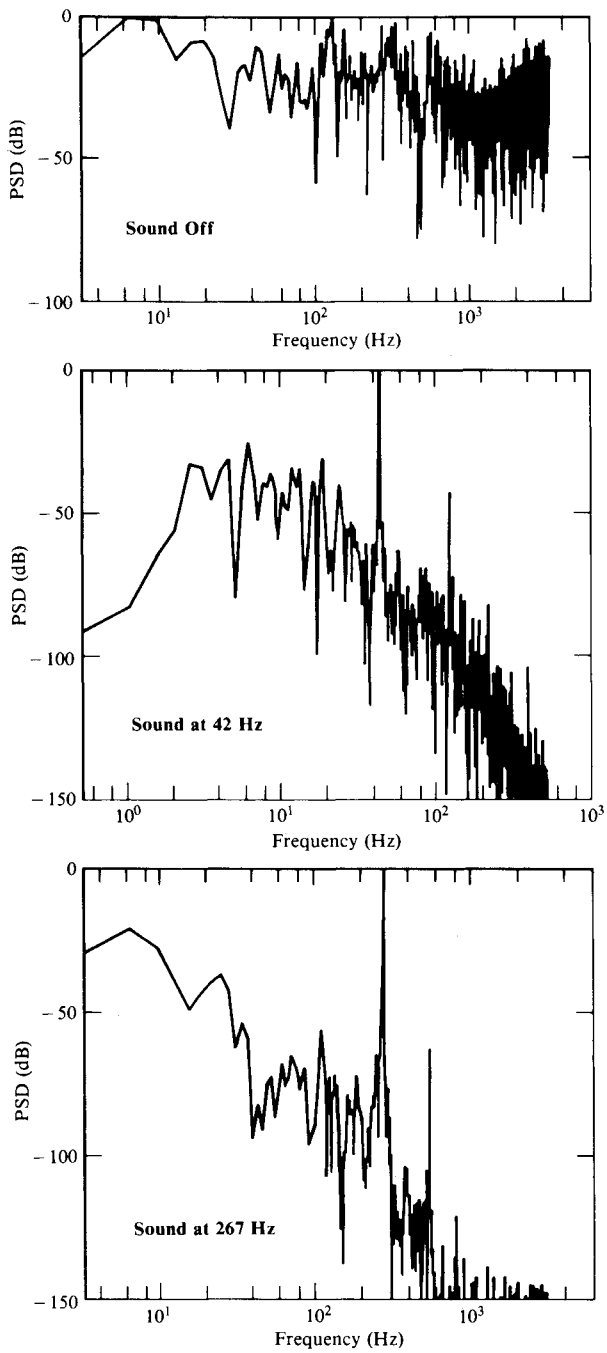

Fig. 5 Frequency spectra from hot wire probe at station 22, $Re_L = 3.15\times10^5$.

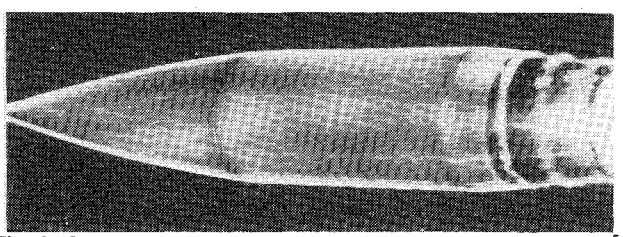

Fig. 6 Smoke-flow visualization over the model at $Re_L = 8.14\times10^5$.

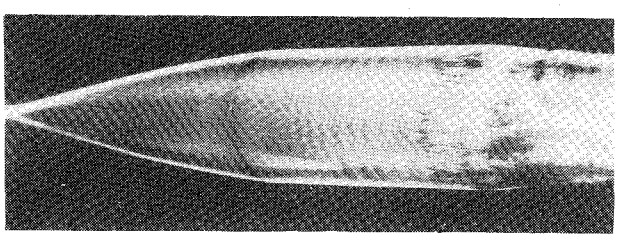

Fig. 7 Smoke-flow visualization over the model at $Re_L = 1.03\times10^6$.

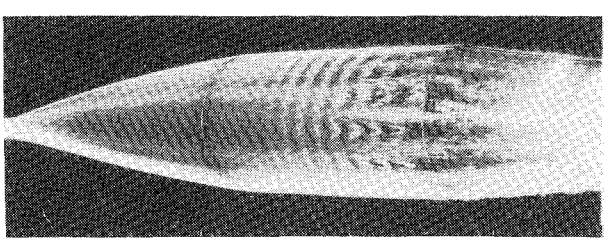

Fig. 8 Sound-induced transition with the sound at 500 Hz, $Re_L = 8.14\times10^5$.

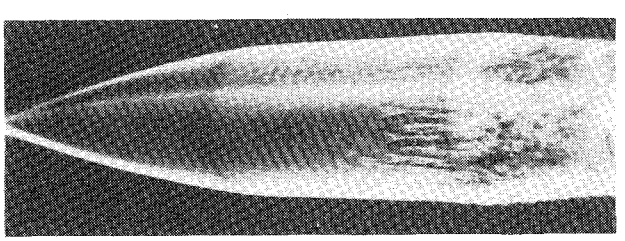

Fig. 9 Sound-induced transition with the sound at 1000 Hz, $Re_L = 8.14\times10^5$.

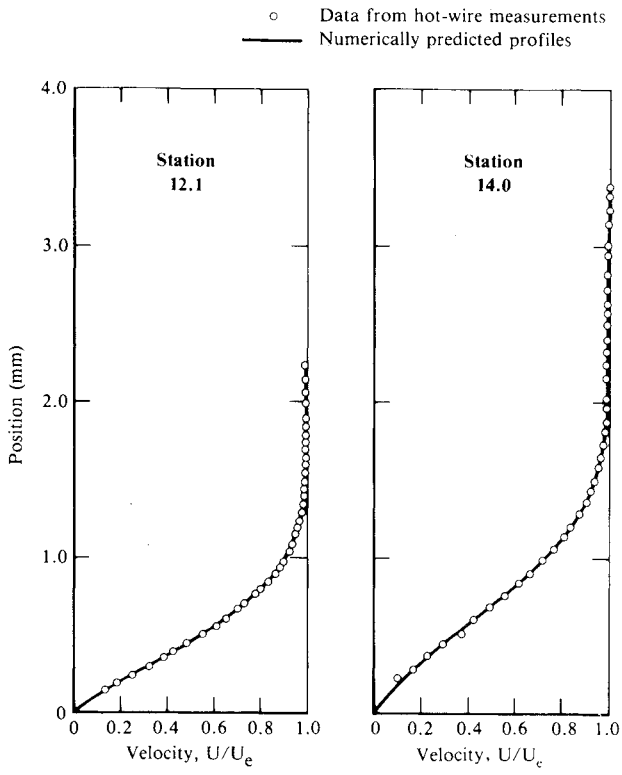

Fig. 10 Comparison of measured boundary-layer profiles with numerically generated profiles.

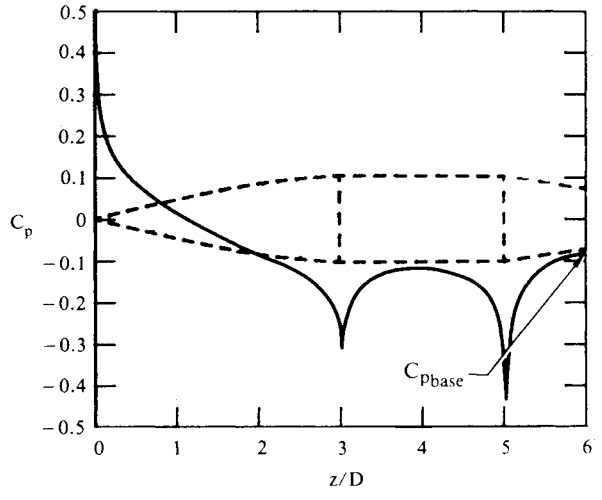

Fig. 11 Pressure distribution along the baseline model at zero angle of attack ($Re_L = 0.814$, 0.928, and 1.030×10^6).

pressure-distribution and boundary-layer profiles vary all along the body, a different neutral stability curve is obtained at each point along the body. It was found that the local Reynolds number does not exceed the critical Reynolds number until just after the nose-midsection junction on the body, where there is an abrupt change from a favorable to an adverse pressure gradient. Three of these neutral stability diagrams are shown in Fig. 12. These neutral curves were generated using the boundary-layer profiles where the pressure distribution suggested that growth of the T-S waves begins (station 12.1, just after the nose-midsection joint), where smoke photographs show the first visible T-S waves (station 14), and where three-dimensional deformation of the boundary layer appears (station 16). The upper and lower limits for which sound could influence the T-S wave formation are also

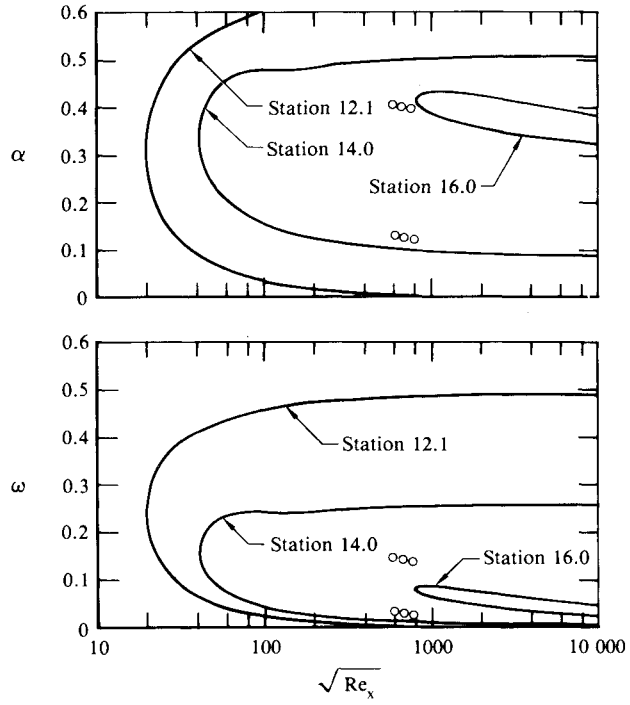

Fig. 12 Neutral stability curves for several stations along the midsection at $Re_L = 8.14 \times 10^5$.

shown in Fig. 12. Apparently, by the time three-dimensional waves become visible in the smoke (station 16), they are in a region where two-dimensional Orr-Sommerfeld theory suggests two-dimensional waves would decay. At this station, the T-S waves have grown too large to be treated by the Orr-Sommerfeld theory.

The ratio of Tollmien-Schlichting wavelength to azimuthal wavelength was almost always ≈ 1.0 suggesting the H-type instability, except occasionally at the lowest frequencies, near the lower branch of the neutral curve. At low frequencies, the ratio of wavelengths was ≈ 0.61, as illustrated in the lower part of Fig. 8. However, this long azimuthal wavelength was observed only occasionally. At low frequencies the Λ vortices were always formed in an aligned fashion indicating the K-type instability, whereas at high frequencies the formation (either aligned or staggered) depended on sound amplitude.

Frequency spectra were obtained from hot-wire data where visual observations indicated the possible existence of a subharmonic. The typical frequency spectra with the hot wire at station 19, 25 mm upstream of the boattail, is shown in Fig. 13. At station 19 with the sound off (Fig. 13a) the frequency spectrum has no strong spikes at any frequency, while the spectra of the hot-wire signal with the sound on (Figs. 13b and 13c) have strong spikes at the excitation frequency of 647 Hz. The spectra of the hot-wire signal with the sound at 106 dB show subharmonics at ≈ 320 Hz that are significantly stronger than any of the higher harmonics. The power of this subharmonic is less than 20 dB below the strength of the fundamental frequency. At station 19 with the sound at 119 dB, the harmonic at 1100 Hz is more than 20 dB stronger than the subharmonic. The presence of a subharmonic where the disturbance amplitude is not significantly greater than the background noise is in agreement with the predictions in Ref. 8.

The hot-wire measurements of the periodic data in Fig. 13 contained only 256 digitized samples. Therefore, similar tests were repeated for an excitation frequency of 740 Hz, where 2048 samples were taken in each string. Smoke photographs, as well as the freestream sound pressure level and fluctuating velocity amplitude, were recorded at a sound level where the Λ vortices were predominantly staggered (C or H type), and

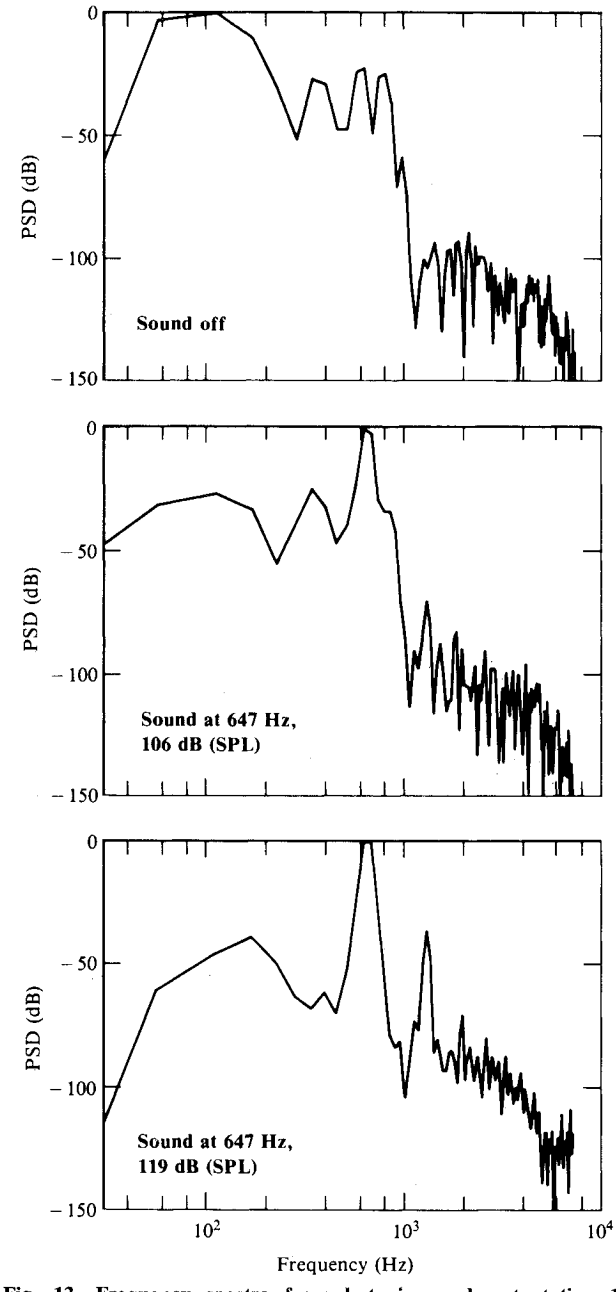

Fig. 13 Frequency spectra from hot-wire probe at station 18, $Re_L = 8.14 \times 10^5$.

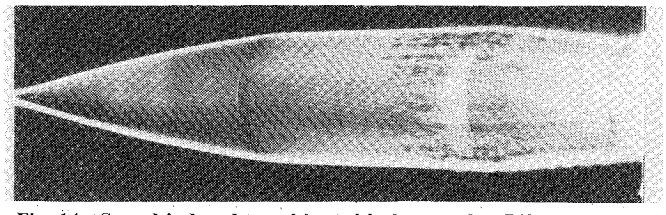

Fig. 14 Sound-induced transition with the sound at 740 Hz, 108 dB, $Re_L = 8.14 \times 10^5$.

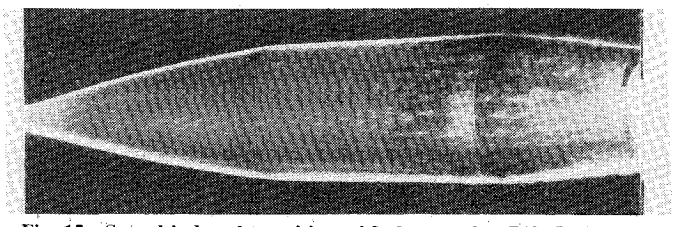

Fig. 15 Sound-induced transition with the sound at 740 Hz, 112 dB, $Re_L = 8.14 \times 10^5$.

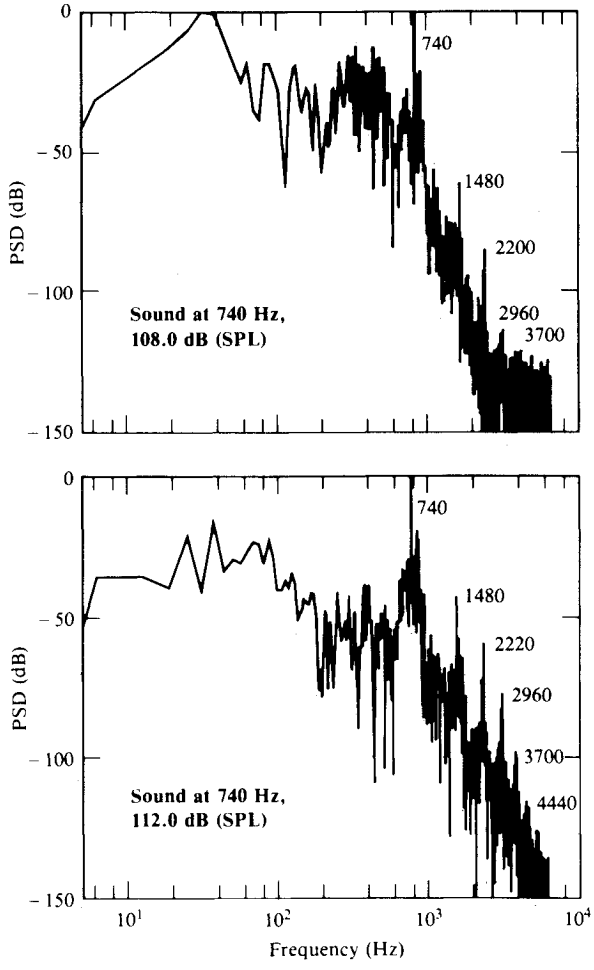

Fig. 16 Frequency spectra from hot-wire probe at station 18, $Re_L = 8.14 \times 10^5$.

again where the sound level was increased just enough to cause the Λ vortices to form in a predominantly aligned fashion (K type). Pictures of the staggered and aligned Λ vortex patterns, shown in Figs. 14 and 15, respectively, were taken during these tests. The amplitude of the fluctuating component of the velocity in the boundary layer was measured just prior to and just after the shift between staggered and aligned Λ vortex formations. The maximum amplitude of the velocity fluctuations in the boundary layer was found to be 1.2% of the freestream velocity. When the sound level was increased until the Λ vortices formed in an aligned fashion, the velocity fluctuations in the boundary layer had an amplitude of 1.5% of the freestream velocity.

The frequency content of the hot-wire signal with a sound amplitude below the threshold, which causes aligned Λ vortex formation, is shown in Fig. 16a. There is no sharp division between the sound amplitude that caused the H-type formation and that which caused the K-type Λ vortices, but there is a gradual shift between the two types of secondary instability as the amplitude increases. The frequency spectrum for the hot-wire signal in the flow with aligned Λ vortices is shown in Fig. 16b. The two plots look quite similar, with the exception of a rise in the spectral power of the frequency near one-half the excitation frequency in the plot with a lower sound level. At frequencies of 250-400 Hz there is significantly greater spectral power at a sound level of 108 dB (Fig. 16a) than at 112 dB (Fig. 16b).

Conclusions

Three transition mechanisms were observed at $Re_L = 8.15 \times 10^5$, which originated as a viscosity-conditioned Tollmien-Schlichting (T-S) instability and depended upon the amplitude and frequency of the acoustic disturbance. During spontaneous transition, i.e., no acoustic enhancement of T-S waves, and for very slight acoustic excitation, T-S waves continuously formed along the midsection and disappeared before reaching the boattail. Transition occurred following separation along the boattail. Generally, the shedding frequency along the boattail was not the same as the T-S wave frequency; however, when sound was used to enhance the T-S wave amplitude, the shedding frequency assumed that of the T-S wave.

When sound was introduced at a single frequency, the three-dimensional response of the T-S waves depended on both the frequency and amplitude of the acoustic disturbance. At low frequencies, the Λ vortices always formed in an aligned fashion. At high frequencies, the Λ vortices appeared in a staggered arrangement when sound was introduced at low amplitudes and in an aligned arrangement when sound was introduced at high amplitudes.

The significance of the present study is that without introducing any subharmonic frequencies, these frequencies develop in the boundary layer provided the fundamental frequency is not significantly stronger than the background disturbances. Furthermore, a nonlinear threshold behavior is demonstrated with respect to Λ-vortex formation, a secondary instability, as a response to disturbance amplitude.

Acknowledgment

This investigation was supported by the U.S. Army Research Office under Grants DAAG 29-78-G-1012 and DAAG 29-80-C-0127.

References

[1]Brown, F.N.M., "The Physical Model of Boundary Layer Transition," *Proceedings of the Ninth Midwestern Mechanics Conference*, University of Wisconsin, Aug. 1965, pp. 421-429.

[2]Knapp, C.F. and Roache, P.J., "A Combined Visual and Hot-Wire Anemometer Investigation of Boundary-Layer Transition," *AIAA Journal*, Vol. 6, Jan. 1968, pp. 29-36.

[3]Kegelman, J.T., Nelson, R.C., and Mueller, T.J., "Smoke Visualization of the Boundary Layer on an Axisymmetric Body," AIAA Paper 79-1635, 1979.

[4]Kegelman, J.T., Nelson, R.C., and Mueller, T.J., "Boundary-Layer and Side-Force Characteristics of a Spinning Axisymmetric Body," AIAA Paper 80-1584-CP, 1980.

[5]Zehentner, R.J., "An Experimental Investigation of the Influence of Nose Bluntness on the Boundary-Layer and Side-Force Characteristics of Spinning Axisymmetric Bodies," Master's Thesis, University of Notre Dame, IN, 1982.

[6]Klebanoff, P.S., Tidstrom, K.D., and Sargent, L.M., "The Three-Dimensional Nature of Boundary-Layer Instability," *Journal of Fluid Mechanics*, Vol. 12, Pt. 1, 1962, pp. 1-34.

[7]Craik, A.D.D., "Nonlinear Resonant Instability in Boundary Layers," *Journal of Fluid Mechanics*, Vol. 50, Pt. 2, 1971, pp. 393-413.

[8]Volodin, A.G. and Zelman, M.B., "The Nature of Differences in Some Forms of Transition in the Boundary Layer," *AIAA Journal*, Vol. 19, July 1981, pp. 950-952.

[9]Herbert, T., "Subharmonic Three-Dimensional Disturbances in Unstable Plane Shear Flows," AIAA Paper 83-1759, 1983.

[10]Kachanov, Y.S., Kozlov, V.V., and Levchenko, V.Y., "Nonlinear Wave Evolution in the Boundary Layer," *Izvestiya Akademii Nauk SSSR, Mechanika Zhidkosti i Gaza*, No. 3, 1977, pp. 49-58.

[11]Saric, W.S., Carter, J.D., and Reynolds, G.A., "Computation and Visualization of Unstable-Wave Streaklines in a Boundary Layer," *Bulletin of the American Physical Society*, Vol. 26, Nov. 1981, p. 1252.

[12]Thomas, A.S.W. and Saric, W.S., "Harmonic and Subharmonic Waves During Boundary-Layer Transition, *Bulletin of the American Physical Society*, Vol. 26, Nov. 1981, p. 1252.

[13]Saric, W.S. and Thomas, A.S.W., "Experiments on the Subharmonic Route to Turbulence in Boundary Layers," *Proceedings of the Symposium on Turbulence and Chaotic Phenomena in Fluids*, Kyoto, Japan, Sept. 1983.

[14]Mueller, T.J., "Smoke Visualization of Subsonic and Supersonic Flows (The Legacy of F.N.M. Brown)," University of Notre Dame, IN, Rept. UNDAS-TN-3412-1, 1979.

[15]Kegelman, J.T., "Experimental Studies of Boundary-Layer Transition on a Spinning and Non-Spinning Axisymmetric Body," Doctoral Dissertation, University of Notre Dame, IN, Sept. 1982.

[16]Cebeci, T. and Bradshaw, P., *Momentum Transfer in Boundary Layers*, McGraw-Hill Book Co., New York, 1977, Chap. 9.